Experimental Implementation of Adiabatic Passage between Different Topological Orders

Xinhua Peng,[1,2,*] Zhihuang Luo,[1] Wenqiang Zheng,[1] Supeng Kou,[3,†] Dieter Suter,[4] and Jiangfeng Du[1,2,‡]
[1]Hefei National Laboratory for Physical Sciences at Microscale and Department of Modern Physics, University of Science and Technology of China, Hefei, Anhui 230026, China
[2]Synergetic Innovation Center of Quantum Information and Quantum Physics, University of Science and Technology of China, Hefei, Anhui 230026, China
[3]Department of Physics, Beijing Normal University, Beijing 100875, China
[4]Fakultät Physik, Technische Universität Dortmund, 44221 Dortmund, Germany
(Received 21 February 2014; published 21 August 2014)

Topological orders are exotic phases of matter existing in strongly correlated quantum systems, which are beyond the usual symmetry description and cannot be distinguished by local order parameters. Here we report an experimental quantum simulation of the Wen-plaquette spin model with different topological orders in a nuclear magnetic resonance system, and observe the adiabatic transition between two Z_2 topological orders through a spin-polarized phase by measuring the nonlocal closed-string (Wilson loop) operator. Moreover, we also measure the entanglement properties of the topological orders. This work confirms the adiabatic method for preparing topologically ordered states and provides an experimental tool for further studies of complex quantum systems.

DOI: 10.1103/PhysRevLett.113.080404 PACS numbers: 03.65.Ud, 03.67.Lx, 64.70.Tg, 76.60.−k

Over the past thirty years, it has become increasingly clear that the Landau symmetry-breaking theory cannot describe all phases of matter and their quantum phase transitions (QPTs) [1–3]. The discovery of the fractional quantum Hall (FQH) effect [4] indicates the existence of an exotic state of matter termed topological orders [5], which are beyond the usual symmetry description. This type of order has some interesting properties, such as robust ground state degeneracy that depends on the surface topology [6], quasiparticle fractional statistics [7], protected edge states [8], topological entanglement entropy [9], and so on. Besides the importance in condensed matter physics, topological orders have also been found to have potential applications in fault-tolerant topological quantum computation [10–12]. Instead of naturally occurring physical systems (e.g., FQH), two-dimensional spin-lattice models, including the toric-code model [10], the Wen-plaquette model [13], and the Kitaev model on a hexagonal lattice [14], were found to exhibit Z_2 topological orders. The study of such systems, therefore, provides an opportunity to understand more features of topological orders and the associated topological QPTs [15–17]. A large body of theoretical work exists on these systems, including several proposals for their physical implementation in cold atoms [18], polar molecules [19], or arrays of Josephson junctions [20]. However, only a very small number of experimental investigations have actually demonstrated such topological properties (e.g., anyonic statistics and robustness) using either photons [21] or nuclear spins [22]. However, in these experiments, specific entangled states having topological properties have been dynamically generated, instead of direct Hamiltonian engineering and ground-state cooling, which are extremely demanding experimentally.

Rather than the toric-code model, the first spin-lattice model with topological orders, here we study an alternative exactly solvable spin-lattice model—the Wen-plaquette model [13]. Two different Z_2 topological orders exist in this system; their stability depends on the sign of the coupling constants of the four-body interaction. Between these two phases, a new kind of phase transition occurs when the couplings vanish. So far, neither these topological orders nor this topological QPT has been observed experimentally. The two major challenges are (i) to engineer and to experimentally control complex quantum systems with four-body interactions and (ii) to detect efficiently the resulting topologically ordered phases. Along the lines suggested by Feynman [23], complex quantum systems can be efficiently simulated on quantum simulators, i.e., programmable quantum systems whose dynamics can be efficiently controlled. Some earlier experiments have been studied, e.g., in condensed-matter physics [21,22,24] and quantum chemistry [25] (see the review on quantum simulation [26] and references therein). Quantum simulations thus offer the possibility to investigate strongly correlated systems exhibiting topological orders and other complex quantum systems that are challenging for simulations on classical computers.

In this Letter, we demonstrate an experimental quantum simulation of the Wen-plaquette model in a nuclear magnetic resonance (NMR) system and observe an adiabatic transition between two different topological orders that are separated by a spin-polarized state. To the best of our knowledge, this is the first experimental observation of such a system based on using the Wilson loop operator, which corresponds to a nonlocal order parameter of a topological QPT [16,17]. Both topological orders are

further confirmed to be highly entangled by quantum state tomography. The experimental adiabatic method paves the way towards constructing and initializing a topological quantum memory [27,28].

We focus on the Wen-plaquette model [13] shown in Fig. 1(a), an exactly solvable quantum spin model with Z_2 topological orders. It is described by the Hamiltonian

$$\hat{H}_{\mathrm{Wen}} = -J\sum_i \hat{F}_i, \tag{1}$$

where $\hat{F}_i = \hat{\sigma}_i^x \hat{\sigma}_{i+\hat{e}_x}^y \hat{\sigma}_{i+\hat{e}_x+\hat{e}_y}^x \hat{\sigma}_{i+\hat{e}_y}^y$ is the plaquette operator that acts on the four spins surrounding a plaquette. Since $\hat{F}_i^2 = 1$, the eigenvalues of $\hat{F}_i$ are $F_i = \pm 1$. We see that when $J > 0$ the ground state has all $F_i = 1$ and when $J < 0$ the ground state has all $F_i = -1$. According to the classification of the projective symmetry group [13], they correspond to two types of topological orders: Z_2A and Z_2B order, respectively. It is obvious that both topological orders have the same global symmetry as that belonging to the Hamiltonian. So one cannot use the concept of "spontaneous symmetry breaking" and the local order parameters to distinguish them. In Z_2A (Z_2B) order, a "magnetic vortex" (or m particle) is defined as $F_i = -1$ ($F_i = 1$) at an even subplaquette and an "electric charge" (or e particle) is defined as $F_i = -1$ ($F_i = 1$) at an odd subplaquette [29]. Because of the mutual semion statistics between e and m particles, their bound states obey fermionic statistics [14,29]. Physically, in Z_2B topological order, a fermionic excitation (the bound state of e and m) sees a π-flux tube around each plaquette and acquires an Aharonov-Bohm phase $e^{i\pi}$ when moving around a plaquette, while in Z_2A topological order, the fermionic excitation feels no additional phase when moving around each plaquette. Thus the transition at $J = 0$ represents a new kind of phase transition that changes quantum orders but not symmetry [13,29].

However, it is difficult to directly observe the transition from Z_2A to Z_2B topological order in the experiment, because the energies of all quantum states are zero at the critical point. Instead, the Wen-plaquette model in a transverse field

$$\hat{H}_{\mathrm{tol}} = \hat{H}_{\mathrm{Wen}} - g\sum_i \hat{\sigma}_i^x. \tag{2}$$

is often studied [15–17]. Without loss of generality, we consider the case $g > 0$. Figure 2 shows its 2D phase diagram, which contains three regions in which the ground state is Z_2B order when $J \ll -g$, Z_2A order when $J \gg g$, and a spin-polarized state without topological order when $|J| \ll g$, respectively. From Fig. 2, we can see that by changing J, the ground state of the system is driven from Z_2A to Z_2B topological order through the trivial spin-polarized state. The spin-polarized region from one topological order to the other one depends on the size of the transverse field strength g: the smaller g is, the narrower the region of the spin-polarized state becomes. If g vanishes (or J is large enough), a QPT occurs between the two types of topological order [13]. The above results are valid only for infinite systems. For finite systems, the situation is more complicated. For example, the topological degeneracies of the system depend on the type of the lattice (even-by-even, even-by-odd, odd-by-odd lattices). However, the properties of the topological orders persist in the Wen-plaquette model with finite-size lattices [13].

The simplest finite system that exhibits topological orders consists of a 2×2 lattice with a periodic boundary condition, as shown in Fig. 1(b). The Hamiltonian can be described as

$$\hat{H}_{\mathrm{Wen}}^4 = -2J(\hat{\sigma}_1^x \hat{\sigma}_2^y \hat{\sigma}_3^x \hat{\sigma}_4^y + \hat{\sigma}_1^y \hat{\sigma}_2^x \hat{\sigma}_3^y \hat{\sigma}_4^x). \tag{3}$$

The fourfold degeneracy of the ground states is a topological degeneracy and the two ground states for $J < 0$ and

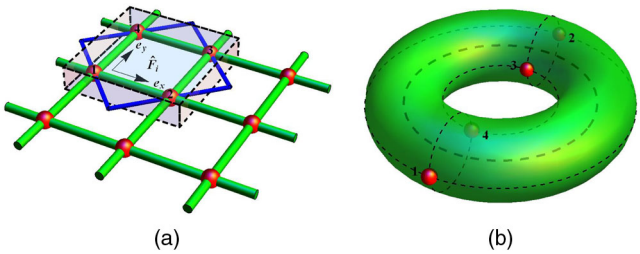

FIG. 1 (color online). (a) Wen-plaquette model. The red spheres represent spin-1/2 particles. The plaquette operator is $\hat{F}_i = \hat{\sigma}_i^x \hat{\sigma}_{i+\hat{e}_x}^y \hat{\sigma}_{i+\hat{e}_x+\hat{e}_y}^x \hat{\sigma}_{i+\hat{e}_y}^y$. The closed string (blue) represents the Wilson loop in a 2×2 lattice. (b) A torus formed from a 2×2 lattice (labeled by 1, 2, 3, and 4) with a periodic boundary condition.

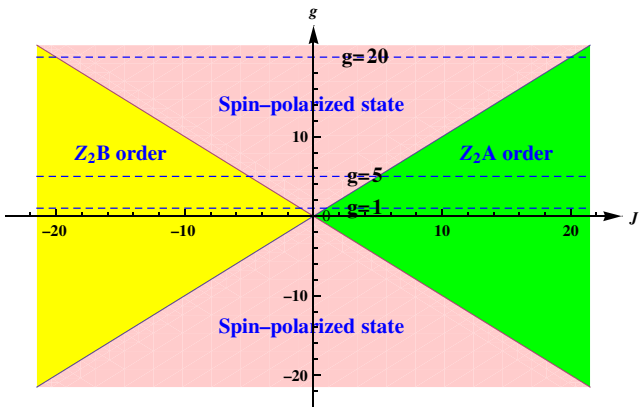

FIG. 2 (color online). Two-dimensional phase diagram of Wen-plaquette model in a transverse field. The yellow, green, and pink regions represent Z_2B topological order, Z_2A topological order, and the spin-polarized state, respectively. The three dashed lines correspond to the tested values of $g = 1$, $g = 5$, and $g = 20$ in the experiment.

for $J > 0$ have different quantum orders [13]. Adding a transverse field, we obtain the transverse Wen-plaquette model $\hat{H}_{\rm tol}$ in Eq. (2) for the finite system, where the degeneracy is partly lifted [15]. For the case $g > 0$, the nondegenerate ground state is

$$|\psi_g\rangle \approx \begin{cases} |\psi_{Z_2B}\rangle = |\phi^+\rangle_{13}|\phi^+\rangle_{24}, & J \ll -g < 0 \\ |\psi_{\rm SP}\rangle = |++++\rangle, & J = 0 \\ |\psi_{Z_2A}\rangle = |\psi^+\rangle_{13}|\psi^+\rangle_{24}, & J \gg g > 0. \end{cases} \quad (4)$$

Here $|\phi^+\rangle = (1/\sqrt{2})(|00\rangle + |11\rangle)$, $|\psi^+\rangle = (1/\sqrt{2})(|01\rangle + |10\rangle)$, and $|+\rangle = (1/\sqrt{2})(|0\rangle + |1\rangle)$. The energy-level diagram and the ground state are given in the Supplemental Material [30]. Equation (4) shows that both topological orders are symmetric and possess bipartite entanglement, while the spin-polarized (SP) state $|\psi_{\rm SP}\rangle$ is a product state without entanglement.

The physical four-qubit system we used in the experiments consists of the nuclear spins in iodotrifluroethylene (C_2F_3I) molecules with one ^{13}C and three ^{19}F nuclei. Figures 3(a) and 3(b) show its molecular structure and relevant properties [30]. The natural Hamiltonian of this system in the doubly rotating frame is

$$\hat{H}_{\rm NMR} = \sum_{i=1}^{4} \frac{\omega_i}{2}\hat{\sigma}_i^z + \sum_{i<j,=1}^{4} \frac{\pi J_{ij}}{2}\hat{\sigma}_i^z\hat{\sigma}_j^z, \quad (5)$$

where ω_i represents the chemical shift of spin i and J_{ij} is the coupling constant. The experiments were carried out on

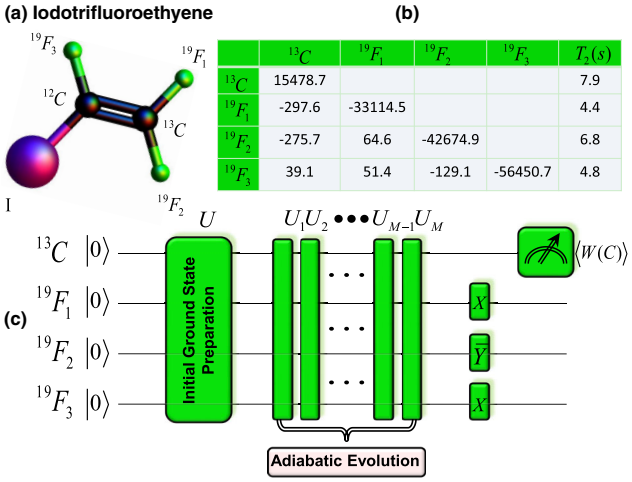

	^{13}C	$^{19}F_1$	$^{19}F_2$	$^{19}F_3$	$T_2(s)$
^{13}C	15478.7				7.9
$^{19}F_1$	-297.6	-33114.5			4.4
$^{19}F_2$	-275.7	64.6	-42674.9		6.8
$^{19}F_3$	39.1	51.4	-129.1	-56450.7	4.8

FIG. 3 (color online). (a) Molecular structure of iodotrifluroethylene. One ^{13}C and three ^{19}F nuclei are used as a four-qubit quantum simulator. (b) Relevant parameters measured at $T = 300$ K. The diagonal and nondiagonal elements represent the chemical shifts and the coupling constants in units of hertz, respectively. The measured spin-lattice relaxation times T_1 are 21 s for ^{13}C and 12.5 s for ^{19}F. (c) Quantum circuit for observing the topological-order transition in the Wen-plaquette model. X and $\bar{Y}$ represent $\pi/2$ rotations of single qubits around the x and $-y$ axes, respectively.

a Bruker AV-400 spectrometer (9.4T) at room temperature $T = 300$ K. The temperature fluctuation was controlled to < 0.1 K, which results in a frequency stability within 1 Hz. Figure 3(c) shows the quantum circuit for the experiment, which can be divided into three steps: (i) preparation of the initial ground state of the Hamiltonian $\hat{H}_{\rm tol}[J(0)]$ for a given transverse field g, (ii) adiabatic simulation of $\hat{H}_{\rm tol}[J(t)]$ by changing the control parameter J from $J(0)$ to $J(T)$, and (iii) detection of the resulting state.

To prepare the system in the ground state, we used the technique of pseudopure states (PPS): $\hat{\rho}_\psi = ((1-\epsilon)/16)\mathbf{I} + \epsilon|\psi\rangle\langle\psi|$, with $\mathbf{I}$ representing the 16×16 identity operator and $\epsilon \approx 10^{-5}$ the polarization. Starting from the thermal state, we prepared the PPS $\hat{\rho}_{0000}$ by line-selective pulses [35]. The experimental fidelity of $\hat{\rho}_{0000}$ defined by $|{\rm Tr}(\hat{\rho}_{\rm th}\hat{\rho}_{\rm expt})|/\sqrt{{\rm Tr}(\hat{\rho}_{\rm th}^2){\rm Tr}(\hat{\rho}_{\rm expt}^2)}$ was around 97.7%. Then we obtained the initial ground state $\hat{\rho}_{\psi_g}$ of $\hat{H}_{\rm tol}[J(0)]$ by a unitary operator realized by the gradient ascent pulse engineering (GRAPE) pulse [36] with a duration of 6 ms.

To observe the ground-state transition, we implemented an adiabatic transfer from $\hat{H}_{\rm tol}[J(0)]$ to $\hat{H}_{\rm tol}[J(T)]$ [37]. The sweep control parameter $J(t)$ was numerically optimized and implemented as a discretized scan with M steps,

$$\hat{U}_{\rm ad} = \prod_{m=1}^{M} \hat{U}_m[J_m] = \prod_{m=1}^{M} e^{-i\hat{H}_{\rm tol}[J_m]\tau}, \quad (6)$$

where the duration of each step is $\tau = T/M$. The adiabatic limit corresponds to $T, M \to \infty, \tau \to 0$. Using $M = 31$, the optimized sweep reaches a theoretical fidelity $> 99.5\%$ of the final state with respect to the true ground state. For each step of the adiabatic passage, we designed the NMR pulse sequence to create an effective Hamiltonian, i.e., $\hat{H}_{\rm tol}[J_m]$ (see the Supplemental Material [30]).

In the experiment, we employed the Wilson loop [16,17,38] to detect the transition between two different topological orders. The effective theory of topological orders is a Z_2 gauge theory and the observables must be gauge invariant quantities. The Wilson loop operator is gauge invariant and can be a nonlocal order parameter. It is defined as $\hat{W}(C) = \prod_C \hat{\sigma}_i^{\alpha_i}$, where the product $\prod_C$ is over all sites on the closed string C, $\alpha_i = y$ if i is even, and $\alpha_i = x$ if i is odd [29]. For the 2×2 lattice system, this corresponds to $\hat{W}(C) = \hat{\sigma}_1^x\hat{\sigma}_2^y\hat{\sigma}_3^x\hat{\sigma}_4^y$. The experimental results of $\langle\hat{W}(C)\rangle$ can be obtained by recording the carbon spectra after a readout pulse $[\pi/2)]_x^{F_1}[\pi/2]_{\bar{y}}^{F_2}[\pi/2]_x^{F_3}$. Figure 4(a) shows the resulting data for three sets of experiments with $g = 1$, $g = 5$, $g = 20$, and J varying from -20 to 20. When $|J/g| \gg 1$, $\langle\hat{W}(C)\rangle$ is close to ± 1, corresponding to Z_2A or Z_2B topological order. The results shown in Fig. 4(a) verify that the transition region becomes narrower and sharper as g decreases. In the absence of the transverse field, $g \to 0$, the ground state makes a sudden transition at $J = 0$ from Z_2B to Z_2A topological order. This

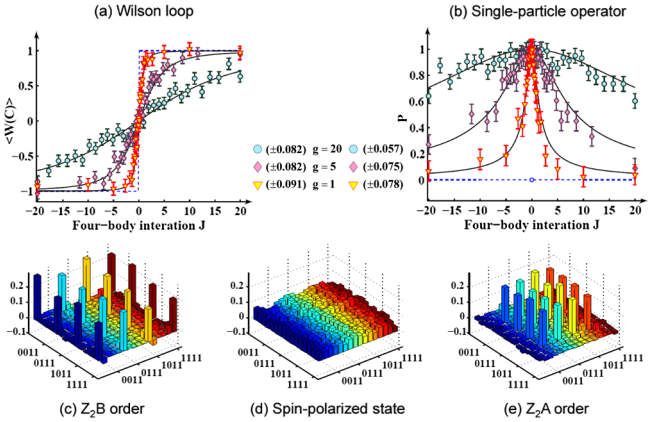

FIG. 4 (color online). (a) Measured expectation values of the nonlocal string operator—the Wilson loop $\langle \hat{W}(C) \rangle$. (b) Measured values P of the local single-particle operator. The experimental points are denoted by the symbols $\triangle$, $\diamond$, and $\circ$ for $g = 1, g = 5$, and $g = 20$, respectively, along with the theoretical expectations denoted by the black solid lines. The error bars indicate the standard deviations of the experimental measurements. The sharp transition denoted by the blue dashed line is the theoretical expectation when $g = 0$. (c)–(e) Real parts of experimentally reconstructed density matrices for the ground states with $g = 1$ at $J = -20$, $J = 0$, and $J = 20$, corresponding to the Z_2B topologically ordered state $|\psi_{Z_2B}\rangle$, the spin-polarized state $|\psi_{\mathrm{SP}}\rangle$, and the Z_2A topologically ordered state $|\psi_{Z_2A}\rangle$. All imaginary parts of the density matrices are small. The rows and columns represent the standard computational basis in binary order, from $|0000\rangle$ to $|1111\rangle$.

is a novel QPT between different topological orders [13]. These results also show that the Wilson loop is a useful nonlocal order parameter that characterizes the different Z_2 topological orders very well.

To demonstrate more clearly that this topological QPT goes beyond the Landau symmetry-breaking theory and cannot be described by local order parameters, we also measured the single-particle operator of the ^{13}C spin,

$$P = |\mathrm{Tr}[\hat{\rho}_f(\hat{\sigma}_1^x - i\hat{\sigma}_1^y)]| = \sqrt{\mathrm{Tr}(\hat{\rho}_f\hat{\sigma}_1^x)^2 + \mathrm{Tr}(\hat{\rho}_f\hat{\sigma}_1^y)^2}.$$

This was performed by measuring the magnitude of the ^{13}C NMR signal while decoupling ^{19}F. Here $\hat{\rho}_f$ is the final state at the end of the adiabatic scan. Because of the symmetry of the Hamiltonian, the values of P are equal for all the four spins. Figure 4(b) shows the experimental results. They are symmetric with respect to $J = 0$, which means that the different Z_2 topological orders cannot be distinguished by the local order parameter.

By performing complete quantum state tomography [39], we reconstructed the density matrices for Z_2B order ($J = -20$), for the spin-polarized state ($J = 0$), and for Z_2A order ($J = 20$) for $g = 1$. The real parts of these density matrices are shown in Figs. 4(c)–4(e). The experimental fidelities are 95.2%, 95.6%, and 95.7%, respectively. From these reconstructed density matrices, we also calculated the entanglement: for both topological orders, $C(\hat{\rho}_{13}^{\mathrm{expt}}) \approx C(\hat{\rho}_{24}^{\mathrm{expt}}) \approx 0.89$, while the others were close to 0; for the spin-polarized state, all $C(\hat{\rho}_{ij}^{\mathrm{expt}})$ are almost zero. Here $\hat{\rho}_{ij}^{\mathrm{expt}}$ is the reduced density matrix of two spins i, j obtained by partially tracing out the other spins from the experimentally reconstructed density matrix $\hat{\rho}^{\mathrm{expt}}$ and the concurrence is defined as $C(\hat{\rho}_{ij}^{\mathrm{expt}}) = \max\{\lambda_1 - \lambda_2 - \lambda_3 - \lambda_4, 0\}$, where the λ_k's (in decreasing order) are the square roots of the eigenvalues of $\hat{\rho}_{ij}^{\mathrm{expt}}(\hat{\sigma}_i^y\hat{\sigma}_j^y)\hat{\rho}_{ij}^{\mathrm{expt}^*}(\hat{\sigma}_i^y\hat{\sigma}_j^y)$ [40]. Therefore, the topological orders exhibit the same bipartite entanglement between qubits 1, 3 and 2, 4 in agreement with Eq. (4). These experimental results are in good agreement with theoretical expectations. The relatively minor deviations can be attributed mostly to the imperfections of the GRAPE pulses, the initial ground state preparation, and the spectral integrals (see the Supplemental Material [30]).

Instead of studying naturally existing topological phases like those in quantum Hall systems, lattice-spin models can be designed to exhibit interesting topological phases. One example is the Wen-plaquette model, which includes many-body interactions. Such interactions have not been found in naturally occurring systems, but they can be generated as effective interactions in quantum simulators. Using a NMR quantum simulator, we provide a first proof-of-principle experiment that implements an adiabatic transition between two different Z_2 topological orders through a spin-polarized state in the transverse Wen-plaquette model. Such models are beyond the Landau symmetry-breaking theory and cannot be described by local order parameters. Reference [17] presented a numerical study of a QPT from a spin-polarized to a topologically ordered phase using a variety of previously proposed QPT detectors and demonstrated their feasibility. Furthermore, we also demonstrated in an experiment that the nonlocal Wilson loop operator can be a nontrivial detector of the topological QPT between different topological orders. This phenomenon requires further investigation to be properly understood.

Although a 2×2 lattice is a very small finite-size system, topological orders exist in the Wen-plaquette model with a periodic lattice of finite size [13]. The validity of the quantum simulation of the topological orders in such a small system also comes from the fairly short-range spin-spin correlations. When $|g/J| \leq 1$, all quasiparticles (the electric charges, magnetic vortices, and fermions) perfectly localize, which leads to a zero spin-spin correlation length [10,41]. Therefore, the topological properties of the ground state persist in such a small system, including the topological degeneracy, the statistics of the quasiparticles, and the nonzero Wilson loop (see the Supplemental Material [30]). The present method can in principle be expanded to larger systems with more spins, which allows one to

explore more interesting physical phenomena, such as lattice-dependent topological degeneracy [13], quasiparticle fractional statistics [7,14], and the robustness of the ground state degeneracy against local perturbations [6,16,17,41]. Quantum simulators using larger spin systems can be more powerful than classical computers and permit the research of topological orders and their physics beyond the capabilities of classical computers. Nevertheless, our present experimental results demonstrate the feasibility of small quantum simulators for strongly correlated quantum systems, and the usefulness of the adiabatic method for constructing and initializing a topological quantum memory.

We thank L. Jiang and C. K. Duan for a helpful discussion. This work is supported by NKBRP (973 Programs No. 2013CB921800, No. 2014CB848700, No. 2012CB921704, and No. 2011CB921803), NNSFC (No. 11375167, No. 11227901, and No. 891021005), SPRB(B) of CAS (No. XDB01030400), and RFDPHEC (No. 20113402110044).

*xhpeng@ustc.edu.cn
†spkou@bnu.edu.cn
‡djf@ustc.edu.cn

[1] S. Sachdev, *Quantum Phase Transition* (Cambridge University Press, Cambridge, England, 1999).
[2] L. D. Landau, Phys. Z. Sowjetunion **11**, 26 (1937).
[3] V. L. Ginzburg and L. D. Landau, J. Exp. Theor. Phys. **20**, 1064 (1950).
[4] D. C. Tsui, H. L. Stormer, and A. C. Gossard, Phys. Rev. Lett. **48**, 1559 (1982); R. B. Laughlin, *ibid.*, **50**, 1395 (1983).
[5] X. G. Wen, Int. J. Mod. Phys. B **04**, 239 (1990).
[6] X.-G. Wen and Q. Niu, Phys. Rev. B **41**, 9377 (1990).
[7] D. Arovas, J. R. Schrieffer, and F. Wilczek, Phys. Rev. Lett. **53**, 722 (1984).
[8] X. G. Wen, Adv. Phys. **44**, 405 (1995).
[9] A. Kitaev and J. Preskill, Phys. Rev. Lett. **96**, 110404 (2006); M. Levin and X. G. Wen, *ibid.* **96**, 110405 (2006).
[10] A. Kitaev, Ann. Phys. (N.Y.) **303**, 2 (2003).
[11] C. Nayak, A. Stern, M. Freedman, and S. Das Sarma, Rev. Mod. Phys. **80**, 1083 (2008).
[12] A. Stern and N. H. Lindner, Science **339**, 1179 (2013).
[13] X. G. Wen, Phys. Rev. Lett. **90**, 016803 (2003).
[14] A. Kitaev, Ann. Phys. (N.Y.) **321**, 2 (2006).
[15] J. Yu, S. P. Kou, and X. G. Wen, Europhys. Lett. **84**, 17004 (2008); S. P. Kou, J. Yu, and X. G. Wen, Phys. Rev. B **80**, 125101 (2009).
[16] A. Hamma and D. A. Lidar, Phys. Rev. Lett. **100**, 030502 (2008).
[17] A. Hamma, W. Zhang, S. Haas, and D. A. Lidar, Phys. Rev. B **77**, 155111 (2008).
[18] L. M. Duan, E. Demler, and M. D. Lukin, Phys. Rev. Lett. **91**, 090402 (2003); X. J. Liu, K. T. Law, and T. K. Ng, Phys. Rev. Lett. **112**, 086401 (2014).
[19] A. Micheli, G. K. Brennen, and P. A. Zoller, Nat. Phys. **2**, 341 (2006).
[20] J. Q. You, X. F. Shi, X. D. Hu, and F. Nori, Phys. Rev. B **81**, 014505 (2010); L. B. Ioffe, M. V. Feigel'man, A. Ioselevich, D. Ivanov, M. Troyer, and G. Blatter, Nature (London) **415**, 503 (2002).
[21] X. C. Yao *et al.*, Nature (London) **482**, 489 (2012); C. Y. Lu, W.-B. Gao, O. Gühne, X.-Q. Zhou, Z.-B. Chen, and J.-W. Pan, Phys. Rev. Lett. **102**, 030502 (2009); J. K. Pachos, W. Wieczorek, C. Schmid, N. Kiesel, R. Pohlner, and H. Weinfurter, New J. Phys. **11**, 083010 (2009).
[22] J. F. Du, J. Zhu, M. G. Hu, and J. L. Chen, arXiv:0712.2694v1; G. R. Feng, G. L. Long, and R. Laflamme, Phys. Rev. A **88**, 022305 (2013).
[23] R. P. Feynman, Int. J. Theor. Phys. **21**, 467 (1982).
[24] X. H. Peng, J. F. Du, and D. Suter, Phys. Rev. A **71**, 012307 (2005); K. Kim, M.-S. Chang, S. Korenblit, R. Islam, E. E. Edwards, J. K. Freericks, G.-D. Lin, L.-M. Duan, and C. Monroe, Nature (London) **465**, 590 (2010); X. H. Peng, J. F. Zhang, J. F. Du, and D. Suter, Phys. Rev. Lett. **103**, 140501 (2009); G. A. Álvarez and D. Suter, Phys. Rev. Lett. **104**, 230403 (2010).
[25] J. F. Du, N. Xu, X. Peng, P. Wang, S. Wu, and D. Lu, Phys. Rev. Lett. **104**, 030502 (2010); B. P. Lanyon *et al.*, Nat. Chem. **2**, 106 (2010); D. W. Lu, N. Xu, R. Xu, H. Chen, J. Gong, X. Peng, and J. Du, Phys. Rev. Lett. **107**, 020501 (2011).
[26] I. M. Georgescu, S. Ashhab, and F. Nori, Rev. Mod. Phys. **86**, 153 (2014).
[27] E. Dennis, A. Kitaev, A. Landahl, and J. Preskill, J. Math. Phys. (N.Y.) **43**, 4452 (2002).
[28] L. Jiang, G. K. Brennen, A. V. Gorshkov, K. Hammerer, M. Hafezi, E. Demler, M. D. Lukin, and P. Zoller, Nat. Phys. **4**, 482 (2008).
[29] X. G. Wen, Phys. Rev. D **68**, 065003 (2003).
[30] See the Supplemental Material at http://link.aps.org/supplemental/10.1103/PhysRevLett.113.080404, which includes Refs. [32–35], for details of the theoretical calculation of the transverse Wen-plaquette model, Eq. (2) (including its energy levels, ground state, and spin-spin correlations), experimental procedure (including the characterization of quantum simulator, the optimization of the adiabatic passage and Hamiltonian simulation), and some auxiliary experimental results including the error analysis.
[31] X. Y. Feng, G. M. Zhang, and T. Xiang, Phys. Rev. Lett. **98**, 087204 (2007).
[32] S. P. Kou, Phys. Rev. Lett. **102**, 120402 (2009).
[33] T. D. W. Claridge, *High Resolution NMR Techniques in Organic Chemistry*, Tetrahedron Organic Chemistry Series 19 (Elsevier, Amsterdam, 1999).
[34] C. H. Tseng, S. Somaroo, Y. Sharf, E. Knill, R. Laflamme, T. Havel, and D. Cory, Phys. Rev. A **61**, 012302 (1999).
[35] X. Peng, X. Zhu, X. Fang, M. Feng, K. Gao, X. Yang, and M. Liu, Chem. Phys. Lett. **340**, 509 (2001).
[36] N. Khaneja, T. Reiss, C. Kehlet, T. Schulte-Herbrüggen, and S. J. Glaser, J. Magn. Reson. **172**, 296 (2005).
[37] A. Messiah, *Quantum Mechanics* (Wiley, New York, 1976).
[38] J. B. Kogut, Rev. Mod. Phys. **51**, 659 (1979).
[39] J. S. Lee, Phys. Lett. A **305**, 349 (2002).
[40] W. K. Wootters, Phys. Rev. Lett. **80**, 2245 (1998).
[41] J. Yu and S. P. Kou, Phys. Rev. B **80**, 075107 (2009).